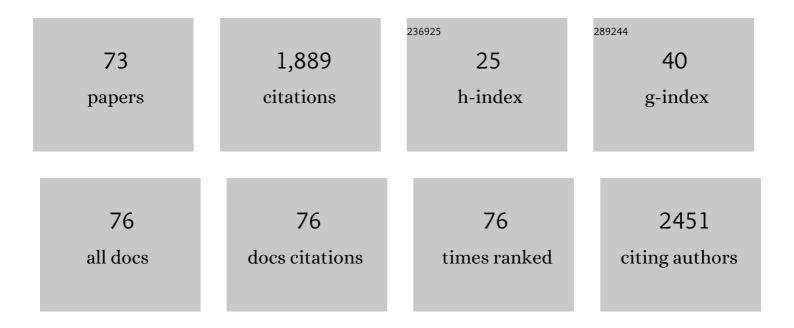
## Masahiro Yanagawa

List of Publications by Year in descending order

Source: https://exaly.com/author-pdf/2831448/publications.pdf Version: 2024-02-01



#	Article	IF	CITATIONS
1	Radiologists with and without deep learning–based computer-aided diagnosis: comparison of performance and interobserver agreement for characterizing and diagnosing pulmonary nodules/masses. European Radiology, 2023, 33, 348-359.	4.5	8
2	Interstitial lung abnormalities are associated with decreased mean telomere length. European Respiratory Journal, 2022, 60, 2101814.	6.7	8
3	Prognostic impact of tumor volume in patients with complete resection of thymoma. Thoracic Cancer, 2022, 13, 1021-1026.	1.9	2
4	Traction Bronchiectasis/Bronchiolectasis on CT Scans in Relationship to Clinical Outcomes and Mortality: The COPDGene Study. Radiology, 2022, 304, 694-701.	7.3	13
5	Diagnostic performance for pulmonary adenocarcinoma on CT: comparison of radiologists with and without three-dimensional convolutional neural network. European Radiology, 2021, 31, 1978-1986.	4.5	10
6	Deep learning algorithm for detection of aortic dissection on non-contrast-enhanced CT. European Radiology, 2021, 31, 1151-1159.	4.5	29
7	Dynamic Chest X-Ray Using a Flat-Panel Detector System: Technique and Applications. Korean Journal of Radiology, 2021, 22, 634.	3.4	22
8	Quantitative volumetry of ground-glass nodules on high-spatial-resolution CT with 0.25-mm section thickness and 1024 matrix: Phantom and clinical studies. European Journal of Radiology Open, 2021, 8, 100362.	1.6	5
9	Progression of traction bronchiectasis/bronchiolectasis in interstitial lung abnormalities is associated with increased all-cause mortality: Age Gene/Environment Susceptibility-Reykjavik Study. European Journal of Radiology Open, 2021, 8, 100334.	1.6	15
10	Greater reductions in blood flow after anti-angiogenic treatment in non-small cell lung cancer patients are associated with shorter progression-free survival. Scientific Reports, 2021, 11, 6805.	3.3	3
11	Prediction of pathological complete response after neoadjuvant chemotherapy in breast cancer: comparison of diagnostic performances of dedicated breast PET, whole-body PET, and dynamic contrast-enhanced MRI. Breast Cancer Research and Treatment, 2021, 188, 107-115.	2.5	13
12	Detectability of pulmonary ossifications in fibrotic lung on ultra-high-resolution CT using 2048 matrix size and 0.25-mm slice thickness. Scientific Reports, 2021, 11, 15119.	3.3	2
13	Spindle Cell Carcinoma of the Breast. Journal of Computer Assisted Tomography, 2021, Publish Ahead of Print, 11-16.	0.9	2
14	Combination of Deep Learning–Based Denoising and Iterative Reconstruction for Ultra-Low-Dose CT of the Chest: Image Quality and Lung-RADS Evaluation. American Journal of Roentgenology, 2020, 215, 1321-1328.	2.2	28
15	The effect of the reconstruction algorithm for the pulmonary nodule detection under the metal artifact caused by a pacemaker. Medicine (United States), 2020, 99, e20579.	1.0	3
16	Traction Bronchiectasis/Bronchiolectasis is Associated with Interstitial Lung Abnormality Mortality. European Journal of Radiology, 2020, 129, 109073.	2.6	38
17	CT Diagnosis of Lung Adenocarcinoma: Radiologic-Pathologic Correlation and Growth Rate. Radiology, 2020, 297, 199-200.	7.3	3
18	Lung Adenocarcinoma at CT with 0.25-mm Section Thickness and a 2048 Matrix: High-Spatial-Resolution Imaging for Predicting Invasiveness. Radiology, 2020, 297, 462-471.	7.3	32

MASAHIRO YANAGAWA

#	Article	IF	CITATIONS
19	Ultra high-resolution computed tomography with 1024-matrix: Comparison with 512-matrix for the evaluation of pulmonary nodules. European Journal of Radiology, 2020, 128, 109033.	2.6	11
20	A case of zonisamide-induced toxic epidermal necrolysis with acute respiratory failure. Allergology International, 2020, 69, 642-644.	3.3	3
21	Influence of field of view size on image quality: ultra-high-resolution CT vs. conventional high-resolution CT. European Radiology, 2020, 30, 3324-3333.	4.5	16
22	Radiogenomics of magnetic resonance imaging and a new multi-gene classifier for predicting recurrence prognosis in estrogen receptor-positive breast cancer. Medicine (United States), 2020, 99, e19664.	1.0	9
23	Spontaneous Regression of Type B3 Thymoma With Mesothelial Cyst. Journal of Thoracic Imaging, 2020, Publish Ahead of Print, W123-W126.	1.5	1
24	Application of deep learning (3-dimensional convolutional neural network) for the prediction of pathological invasiveness in lung adenocarcinoma. Medicine (United States), 2019, 98, e16119.	1.0	21
25	Imaging Patterns Are Associated with Interstitial Lung Abnormality Progression and Mortality. American Journal of Respiratory and Critical Care Medicine, 2019, 200, 175-183.	5.6	142
26	Ultra-low-dose chest computed tomography for interstitial lung disease using model-based iterative reconstruction with or without the lung setting. Medicine (United States), 2019, 98, e15936.	1.0	11
27	Quantitative Computed Tomography Imaging of Lung Cancer. Japanese Journal of Lung Cancer, 2019, 59, 29-36.	0.1	Ο
28	Influence of gantry rotation time and scan mode on image quality in ultra-high-resolution CT system. European Journal of Radiology, 2018, 103, 71-75.	2.6	14
29	Effect of Matrix Size on the Image Quality of Ultra-high-resolution CT of the Lung. Academic Radiology, 2018, 25, 869-876.	2.5	108
30	Radiologic–Pathologic Correlation of Solid Portions on Thin-section CT Images in Lung Adenocarcinoma: A Multicenter Study. Clinical Lung Cancer, 2018, 19, e303-e312.	2.6	43
31	Volumetric analysis of the thymic epithelial tumors: correlation of tumor volume with the WHO classification and Masaoka staging. Journal of Thoracic Disease, 2018, 10, 5822-5832.	1.4	10
32	Pulmonary Emphysema Quantification on Ultra–Low-Dose Computed Tomography Using Model-Based Iterative Reconstruction With or Without Lung Setting. Journal of Computer Assisted Tomography, 2018, 42, 760-766.	0.9	5
33	Subjective and objective comparisons of image quality between ultra-high-resolution CT and conventional area detector CT in phantoms and cadaveric human lungs. European Radiology, 2018, 28, 5060-5068.	4.5	78
34	Classification of idiopathic interstitial pneumonias using anti–myxovirus resistance-protein 1 autoantibody. Scientific Reports, 2017, 7, 43201.	3.3	14
35	Pleural abnormalities in the Framingham Heart Study: prevalence and CT image features. Occupational and Environmental Medicine, 2017, 74, 756-761.	2.8	11
36	The <i>MUC5B</i> promoter polymorphism is associated with specific interstitial lung abnormality subtypes. European Respiratory Journal, 2017, 50, 1700537.	6.7	55

MASAHIRO YANAGAWA

#	Article	IF	CITATIONS
37	Radiological prediction of tumor invasiveness of lung adenocarcinoma on thin-section CT. Medicine (United States), 2017, 96, e6331.	1.0	33
38	Quantitative pulmonary blood flow measurement using 15O-H2O PET with and without tissue fraction correction: a comparison study. EJNMMI Research, 2017, 7, 102.	2.5	6
39	Submillisievert CT using model-based iterative reconstruction with lung-specific setting: An initial phantom study. European Radiology, 2016, 26, 4457-4464.	4.5	12
40	Dual-energy dynamic CT of lung adenocarcinoma: correlation of iodine uptake with tumor gene expression. European Journal of Radiology, 2016, 85, 1407-1413.	2.6	18
41	Ultra-High-Resolution Computed Tomography of the Lung: Image Quality of a Prototype Scanner. PLoS ONE, 2015, 10, e0137165.	2.5	92
42	Predicting adenocarcinoma recurrence using computational texture models of nodule components in lung CT. Medical Physics, 2015, 42, 2054-2063.	3.0	38
43	Diameter of Solid Tumor Component Alone Should be Used to Establish T Stage in Lung Adenocarcinoma. Annals of Surgical Oncology, 2015, 22, 1318-1323.	1.5	30
44	Paradoxical signal pattern of mediastinal cysts on T2-weighted MR imaging: phantom and clinical study. European Journal of Radiology, 2014, 83, 1016-1021.	2.6	4
45	Prognostic Importance of Volumetric Measurements in Stage I Lung Adenocarcinoma. Radiology, 2014, 272, 557-567.	7.3	46
46	Pathologically Proved Nonspecific Interstitial Pneumonia: CT Pattern Analysis as Compared with Usual Interstitial Pneumonia CT Pattern. Radiology, 2014, 272, 549-556.	7.3	57
47	Ultra-low-dose CT of the Lung. Academic Radiology, 2014, 21, 695-703.	2.5	42
48	The Effect of the Virtual Monochromatic Spectral Imaging for the Metallic Artifact and the Pulmonary Nodule Detection. Journal of Computer Assisted Tomography, 2013, 37, 707-711.	0.9	7
49	Evaluation of Response to Neoadjuvant Chemotherapy for Esophageal Cancer: PET Response Criteria in Solid Tumors Versus Response Evaluation Criteria in Solid Tumors. Journal of Nuclear Medicine, 2012, 53, 872-880.	5.0	89
50	Pulmonary nodules: Effect of adaptive statistical iterative reconstruction (ASIR) technique on performance of a computer-aided detection (CAD) system—Comparison of performance between different-dose CT scans. European Journal of Radiology, 2012, 81, 2877-2886.	2.6	36
51	Usual interstitial pneumonia and nonspecific interstitial pneumonia: Correlation between CT findings at the site of biopsy with pathological diagnoses. European Journal of Radiology, 2012, 81, 2919-2924.	2.6	11
52	Intratumoral heterogeneity of F-18 FDG uptake differentiates between gastrointestinal stromal tumors and abdominal malignant lymphomas on PET/CT. Annals of Nuclear Medicine, 2012, 26, 222-227.	2.2	48
53	Prediction of Thymoma Histology and Stage by Radiographic Criteria. Thoracic Surgery Clinics, 2011, 21, 1-12.	1.0	32
54	Detection of pulmonary nodules by C-arm CT using a phantom lung: comparison with CT. Acta Radiologica, 2011, 52, 964-968.	1.1	8

Masahiro Yanagawa

#	Article	IF	CITATIONS
55	Multidetector CT of the Lung: Image Quality with Garnet-based Detectors. Radiology, 2010, 255, 944-954.	7.3	26
56	Adaptive Statistical Iterative Reconstruction Technique for Pulmonary CT. Academic Radiology, 2010, 17, 1259-1266.	2.5	59
57	Automated assessment of malignant degree of small peripheral adenocarcinomas using volumetric CT data: Correlation with pathologic prognostic factors. Lung Cancer, 2010, 70, 286-294.	2.0	49
58	CT-guided Percutaneous Cutting Needle Biopsy of Thymic Epithelial Tumors. Academic Radiology, 2010, 17, 772-778.	2.5	4
59	One-dimensional quantitative evaluation of peripheral lung adenocarcinoma with or without ground-glass opacity on thin-section CT images using profile curves. British Journal of Radiology, 2009, 82, 532-540.	2.2	23
60	Volume of pulmonary lobes and segments in chronic obstructive pulmonary diseases calculated using newly developed three-dimensional software. Japanese Journal of Radiology, 2009, 27, 115-122.	2.4	11
61	Thin-section CT of lung without ECG gating: 64-detector row CT can markedly reduce cardiac motion artifact which can simulate lung lesions. European Journal of Radiology, 2009, 69, 102-107.	2.6	11
62	Nonspecific interstitial pneumonia: Histologic correlation with high-resolution CT in 29 patients. European Journal of Radiology, 2009, 70, 35-40.	2.6	19
63	Doubling time of lung cancer determined using three-dimensional volumetric software: Comparison of squamous cell carcinoma and adenocarcinoma. Lung Cancer, 2009, 66, 211-217.	2.0	53
64	Commercially Available Computer-Aided Detection System for Pulmonary Nodules on Thin-Section Images Using 64 Detectors-Row CT. Academic Radiology, 2009, 16, 924-933.	2.5	38
65	Computed Tomography Values Calculation and Volume Histogram Analysis for Various Computed Tomographic Patterns of Diffuse Lung Diseases. Journal of Computer Assisted Tomography, 2009, 33, 731-738.	0.9	19
66	Nonspecific Interstitial Pneumonia Associated with Collagen Vascular Disease: Analysis of CT Features to Distinguish the Various Types. Internal Medicine, 2009, 48, 753-761.	0.7	20
67	Acute eosinophilic pneumonia: Thin-section CT findings in 29 patients. European Journal of Radiology, 2008, 65, 462-467.	2.6	84
68	Heterologous carcinosarcoma of Douglas' pouch with adenocarcinomas of the fallopian tube and the peritoneal cavity. Pathology, 2008, 40, 641-645.	0.6	4
69	Pulmonary Nodules: 3D Volumetric Measurement with Multidetector CT—Effect of Intravenous Contrast Medium. Radiology, 2007, 245, 881-887.	7.3	33
70	Solitary pulmonary metastases from renal cell carcinoma: comparison of high-resolution CT with pathological findings. Radiation Medicine, 2006, 24, 680-686.	0.8	3
71	Imaging characteristics of papillary renal cell carcinoma by computed tomography scan and magnetic resonance imaging. International Journal of Urology, 2005, 12, 795-800.	1.0	35
72	Artificial Intelligence Improves Radiologist Performance for Predicting Malignancy at Chest CT. Radiology, 0, , .	7.3	0

#	Article	IF	CITATIONS
73	Visualization of the Associations between the CT Features Extracted from a Deep Learning Survival Prediction Model and Histopathologic Risk Factors. Radiology, 0, , .	7.3	Ο